ADVANCED ENERGY MATERIALS
www.advenergymat.de

Influence of Silicon Nanoscale Building Blocks Size and Carbon Coating on the Performance of Micro-Sized Si–C Composite Li-Ion Anodes

*Ran Yi, Fang Dai, Mikhail L. Gordin, Hiesang Sohn, and Donghai Wang**

Silicon has been intensively pursued as the most promising anode material for Li-ion batteries due to its high theoretical capacity of 3579 mAh/g. Micro-sized Si–C composites composed of nanoscale primary building blocks are attractive Si-based anodes for practical application because they not only achieve excellent cycling stability, but also offer both gravimetric and volumetric capacity. However, the effects of key parameters in designing such materials on their electrochemical performance are unknown and how to optimize them thus remains to be explored. Herein, the influence of Si nanoscale building block size and carbon coating on the electrochemical performance of the micro-sized Si–C composites is investigated. It is found that the critical Si building block size is 15 nm, which enables a high capacity without compromising the cycling stability, and that carbon coating at higher temperature improves the first cycle coulombic efficiency (CE) and the rate capability. Corresponding reasons underlying electrochemical performance are revealed by various characterizations. Combining both optimized Si building block size and carbon coating temperature, the resultant composite can sustain 600 cycles at 1.2 A/g with a fixed lithiation capacity of 1200 mAh/g, the best cycling performance with such a high capacity for micro-sized Si-based anodes.

1. Introduction

The development of electric vehicles (EV) and plug-in hybrid electric vehicles (PHEV) requires batteries with high energy density and long cycle lives.[1,2] Li-ion batteries (LIBs) are the dominant candidate for these applications.[3] Current commercial graphite anodes for Li-ion batteries have a theoretical capacity of 372 mAh/g.[4] As increasing anode capacity is one key means of increasing LIBs' energy density, new anode materials based on abundant, high-capacity silicon (theoretical capacity of 3579 mAh/g) have drawn significant attention as promising alternatives to graphite.[5] However, Si undergoes a large volume change during the lithiation and delithiation processes, causing severe pulverization of Si particles, an unstable solid-electrolyte interphase (SEI) layer, and structural degradation of the electrode–all of which can lead to poor cycling stability.[6,7] Numerous efforts have been made to address these issues, with the main focus on development of Si-based nanomaterials, such as nanowires, nanosprings, nanotubes, and nanoparticles.[8–16] Though Si-based nanomaterials offer high gravimetric capacity and long cycle lifetime, they suffer from intrinsically low tap density, leading to low volumetric capacity,[17] and from expensive preparation which makes large-scale manufacturing difficult.[18–20] Recent work by several researchers has thus focused on materials that combine the advantages of both size regimes, featuring micro-sized particles composed of nanoscale Si building blocks to achieve both high volumetric capacity and stable cycling.[21–24] Especially, SiO provides an ideal platform for preparation of micro-sized anodes with excellent performance such as carbon-coated porous SiO,[25] TiO_2-coated SiO,[26] and SiO-C composite.[27] Besides, thermal disproportionation of SiO proved to be an effective strategy to further improve the performance of micro-sized Si-based anodes.[28–30] For example, Park et al. reported a micro-sized carbon-coated Si-based multicomponent anode composed of Si/SiO cores and crystalline SiO_2 shells that showed a high reversible capacity and good cycling stability.[29] A porous Si-based multicomponent system was developed by Choi and Park et al. through a metal-assisted catalytic etching approach followed by a chemical-assisted thermal disproportionation process. The composite exhibited a stable retention over 100 cycles with a high capacity.[30] We previously demonstrated a micro-sized Si–C composite composed of interconnected Si and carbon nanoscale building blocks via a low-cost and scalable route using SiO as starting materials.[31] The Si building blocks are small enough to avoid significant fracture during volume change, while the uniformly distributed carbon ensures high utilization of silicon even when the micro-sized particles crack upon cycling. The composite thus exhibits excellent cycling stability and rate capability, along with a high volumetric capacity due to the high packing of primary particles within the micro-sized particles. However, the 1st cycle coulombic efficiency (CE) is just 77%, and contribution of Si to the specific capacity of the composite is only around 1930 mAh/g, much lower than the theoretical capacity of Si (3579 mAh/g), so further work to improve the material is still needed.

R. Yi, Dr. F. Dai, M. L. Gordin, Dr. H. Sohn, Prof. D. Wang
Department of Mechanical and Nuclear Engineering
The Pennsylvania State University
University Park, PA 16802, USA
E-mail: dwang@psu.edu

DOI: 10.1002/aenm.201300496

There are several key parameters that can be tuned in designing such a material. Due to their high volume change, Si building blocks should be kept small enough to prevent serious cracking and thus enable stable cycling. However, smaller building blocks are accompanied by a larger surface area; even a thin layer of natural oxides (SiO_2 and SiO_x with $0 < x < 2$) would result in a high content of impurities for the whole material, leading to low 1st coulombic efficiency and low specific capacity.[32] Because of this tradeoff, it is necessary to find out the optimized size of Si building blocks to achieve a high capacity without compromising the cycling stability of the composite. Although there are several reports that correlate the effects of particle size to electrochemical performance of Si nanoparticles,[33–35] to the best of our knowledge, no studies are available on the effect of Si building block size within a micro-sized Si–C composite anode material on its electrochemical performance. Our current synthetic route offers the opportunity to study this effect, since Si building block size can be easily controlled by tuning the thermal disproportionation temperature of SiO, the Si precursor.

Carbon coating also plays an important role in improving the performance of Si-based anodes by increasing electrical conductivity, helping the formation of a better SEI layer, and providing buffer layer for the volume change of Si.[36–38] Deposition of carbonaceous gases (C_2H_2, C_3H_6, etc) has proved to be an especially effective carbon coating method, particularly for porous Si precursors,[23,39,40] for which depositing a thin, conformal coating is usually challenging if other methods are employed. Additionally, carbonaceous gases are reducing agents at high temperature[41] and can potentially reduce SiO_x, thereby improving performance. It has been demonstrated by the study of $LiFePO_4$/C composites that sp^2/sp^3 and D/G ratios of carbon prominently affect electrochemical performance.[42] However, despite the wide range of temperatures[23,39,40,43] and thus resultant structures reported for carbon deposition on Si, the influence of carbon coating temperature on the performance of Si–C composites has not been intensively studied.

Herein, we investigate both the influence of the Si building block size on the performance of micro-sized Si–C composites and the role that carbon coating temperature plays in improving the performance of the composite with the optimized building block size. It has been found that 15 nm is the critical building block size, striking a delicate balance between cycling stability and reversible capacity. On the other hand, carbon coating at higher temperature helps to improve the 1st CE and the rate capability by reducing more SiO_x ($0 < x < 2$) and forming higher-quality carbon. By combining the optimized nanoscale building blocks and carbon coating, we demonstrate that the resultant composite can sustain 600 cycles at 1.2 A/g with a fixed lithiation capacity of 1200 mAh/g.

2. Results and Discussion

2.1. Influence of the Si Building Block Size on the Electrochemical Performance of Si–C Composites

Three porous Si samples were prepared by thermal disproportionation of SiO at three different temperatures (1100 °C, 1300 °C, and 1400 °C) followed by etching with hydrofluoric acid, and were used as precursors for Si–C composites. To exclude the influence of carbon quality and amount, carbon deposition was carried out at the same temperature of 620 °C and the acetylene flow rate was controlled to obtain three Si–C composites with similar carbon contents of around 20 wt% by elemental analysis. The materials disproportionated at 1100 °C, 1300 °C, and 1400 °C were designated Si-1100-620, Si-1300-620, and Si-1400-620, respectively. For comparison, the material disproportionated at 950 °C[31] (named Si-950-620) is included in the following discussion. The phase and crystallinity of the three materials were examined by X-ray diffraction (XRD). As shown in **Figure 1**a, the peaks of all patterns can be indexed to those of crystalline face-centered cubic Si (JCPDS Card No.27-1402). The peaks become narrower as temperature increases, indicating increased crystalline domain size. The morphology, structure, and size of the Si–C composites were investigated by scanning electron microscopy (SEM) and transmission electron microscopy (TEM). All samples are composed of micro-sized particles with a size of up to 30 μm (Figure 1b), similar to the SiO precusor (Figure S1 in the Supporting Information (SI)), suggesting the microsize nature has been well inherited. However, while Si-1100-620 and Si-1300-620 were irregularly-shaped particles, the Si-1400-620 particles were instead rounded (Figure S2a), which may be due to further growth of particles at higher temperature. The difference in building block size is revealed by TEM. All samples are composed of interconnected Si nanoparticles, however, the particle size increases from 10 nm for Si-950[31] to 15 nm for Si-1100, to 30 nm for Si-1300, and further to 80 nm for Si-1400, as shown in Figure 1c-f and Figure S2b-d. Correspondingly, the carbon layer on each building block becomes thicker as the particle size increases and surface area commensurately decreases.

Galvanostatic charging/discharging was employed to evaluate the electrochemical performance of all Si–C composites as Li-ion anode materials. The initial voltage profiles at a current density of 400 mA/g are shown in **Figure 2**a. The initial discharge and charge capacities of Si-1100-620 are 2519 and 1962 mAh/g, respectively, giving a first cycle CE of 78%. Si-1300-620 delivers initial discharge and charge capacities of 2752 and 2253 mAh/g, respectively, corresponding to a first CE of 82%. Si-1400-620 exhibits a higher CE of 84%, with discharge and charge capacities of 3312 and 2778 mAh/g, respectively. Although it has a lower initial capacity and initial CE, Si-1100-620 shows stable cyclability at 1 A/g with the 1st cycle activated at 400 mA/g (Figure 2b). A capacity of 1800 mA/g was obtained after 100 cycles with no noticeable capacity fading compared to the discharge capacity of the second cycle. In contrast, the capacity of Si-1300-620 was only stable for 20 cycles and then started to fade quickly. Si-1400-620 showed the worst cycling stability, as the capacity fading happened at the very beginning.

Given the carbon content of around 20 wt% and neglecting the capacity of carbon, the specific capacity based only on the mass of Si in the composites is 2452, 2816, and 3472 mAh/g for Si-1100-620, Si-1300-620, and Si-1400-620, respectively. While the capacity of Si in Si-1400-620 is close to the theoretical value, the capacity of Si in Si-1100-620 is far from that. As found in our previous study, silicon oxides (SiO_2 and SiO_x with $0 < x < 2$) exist in porous Si due to natural oxidization.[31] These oxides

Adv. Energy Mater. 2013,
DOI: 10.1002/aenm.201300496

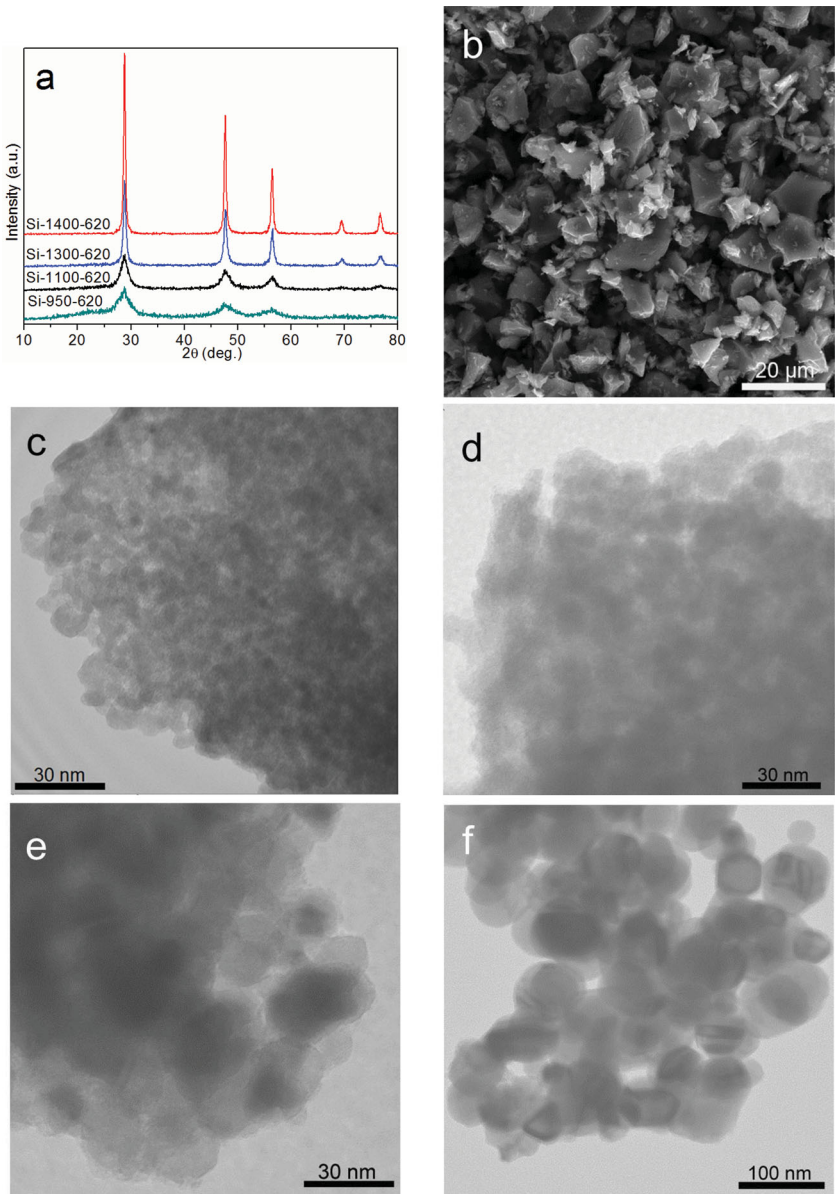

Figure 1. (a) XRD patterns of Si-950-620, Si-1100-620, Si-1300-620 and Si-1400-620. (b) Typical SEM image of Si-1100-620 and Si-1300-620, and TEM images of (c) Si-950-620, (d) Si-1100-620, (e) Si-1300-620 and (f) Si-1400-620. XRD pattern and TEM image of Si-950-620 are reproduced from ref. [31] for comparison.

lead to lower reversible capacity and 1st cycle CE not only because of the dead weight of inactive SiO_2, but also because of the irreversible formation of Li_2O and Li_4SiO_4 during the initial lithiation of SiO_x.[32] In addition, Li_2O and Li_4SiO_4 could act as a constraining shell that limits the expansion and thus the extent of lithiation of Si core by introducing compressive stress, further decreasing reversible capacity.[44] However, despite lower capacity, the presence of surface oxides may improve the cycling stability as demonstrated in a previous report.[45] A larger surface area should result in a higher content of silicon oxides. The specific surface area, reversible capacity, 1st cycle CE and cyclability of the three samples are summarized in **Table 1**. Among the three porous samples, Si-1100-620 has the highest surface area due to its smallest particle size. It is clear that the reversible capacity and the 1st CE are directly related to the Si building block size and inversely related to the surface area, whereas the cycling becomes more stable as the building block size decreases. The result of our previous study,[31] in which the Si–C composite (Si-950-620) with 10 nm Si building blocks showed a reversible capacity of 1930 mAh/g (based on the mass of Si in the composite) and a 1st CE of 77%, is consistent with this trend.

To better understand the different cyclabilities of the Si–C composites with different building block sizes, SEM and TEM analyses were carried out on delithiated Si–C composite electrodes after 100 cycles. In the case of Si-1100-620, despite the cracks shown in **Figure 3**a, contours of single particles can clearly be seen in the high magnification image in Figure 3b, indicating that growth of the SEI layer has been efficiently limited. In comparison, parts of the Si-1300-620 electrode (Figure 3c) and nearly all of the Si-1400-620 electrode (Figure 3d) are buried under a thick SEI layer, which suggests unstable SEI growth during cycling. It should be noted that severe charging as a result of the insulating nature of SEI layer prevented us from obtaining clear high-magnification images for Si-1300-620 and Si-1400-620 electrodes. Additionally, much of the active material on the Si-1400-620 electrode was found to have peeled away from the current collector after cycling. The differences mentioned above serve as strong evidence that Si–C composites with smaller building blocks can much more effectively mitigate the unstable growth of the SEI layer upon cycling. Insight at the nanoscale level was gained by TEM. Because Super P is similar in size (Figure S4) to the building blocks of Si-1300-620 and Si-1400-620 and would not degrade upon cycling, electrodes for postmortem TEM observation were prepared without Super P (Si–C composite and binder in an 8:2 ratio). The electrolyte, SEI layer, and binder were removed by washing with acetonitrile and 1 M hydrochloric acid solution. The morphology and interconnectedness of the building blocks are similar to those of the pristine composites, except that the size of Si slightly increased (Figure 3e-g), consistent with the previous in-situ study of Si nanoparticles.[46] However, as mentioned previously, when opening the cells we found that a large part of the active material on the Si-1400-620 electrode was peeling off of the current collector, while the Si-1100-620 and Si-1300-620 electrodes appeared largely intact.

Based on the cycling performance and the SEM and TEM analyses after cycling, we propose that the core mechanisms by which volume change of micro-sized Si–C composites

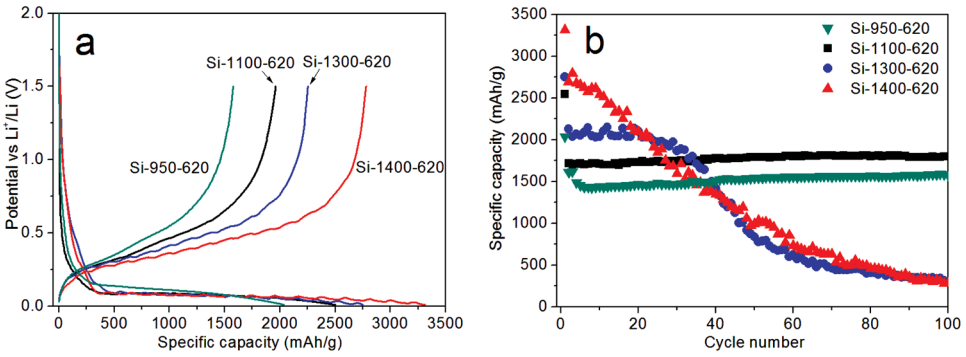

Figure 2. First cycle voltage profiles and cycling performance of Si-950-620, Si-1100-620, Si-1300-620 and Si-1400-620. Specific capacities are calculated based on the weight of Si–C composites. Voltage profile and cycling performance of Si-950-620 are reproduced from ref. [31] for comparison.

affects cyclability is by influencing SEI growth and electrode structural integrity, as schematically shown in **Figure 4**. Large volume change can break the SEI layer and expose fresh material to the electrolyte, leading to continual SEI growth. As the SEI layer grows, it will increase cell impedance by both raising the barrier to Li^+ ion diffusion and electrically insulating particles of the composite from one another, and may eventually consume enough electrolyte to kill the cell.[6] The larger SEI layers on larger Si–C building blocks are particularly vulnerable to breaking during volume change of the underlying silicon, as larger nanoparticles have been shown to release more energy when cracking and thus be more prone to it.[47] A robust SEI layer is formed on the surface of Si-1100-620 during the initial cycle and remains stable in later cycles due to the small size of the Si building blocks. The SEI stability is evidenced by the average CE of 99.76% from the 2nd to 100th cycles (Figure S5), among the best for published Si anodes.[11] Although the Si building blocks of Si-1300-620 do not themselves break, their SEI layer cracks as the Si expands and contracts, inducing the formation of new SEI by exposing fresh Si surface to electrolyte. The continuous formation of SEI is verified by the low coulombic efficiency of around 98% even while the capacity was stable (Figure S5). As the SEI grows thicker, the electrical contact between particles and lithium diffusion to particles decrease and likely hit a critical value, leading to capacity fading after 20 cycles. With the largest building blocks, Si-1400-620 has the worst situation. The SEI layer becomes even more unstable, with CE of about 97% (Figure S5), and the electrode also undergoes fast structural degradation – evidenced by its severe peel-off after cycling – resulting in capacity fading at the very beginning due to the loss of electrical contact.

2.2. Influence of Carbon Coating on the Electrochemical Performance of the Si–C Composite

To determine the influence of carbon coating on the performance of Si–C composites, carbon-coating was also performed at a higher temperature. The Si material prepared at 1100 °C was chosen for this study due to its stable cyclability. The acetylene deposition was carried out at 800 °C with a controlled flow rate to obtain a new composite, namely Si-1100-800, with the similar carbon content (about 20 wt% by elemental analysis) to Si-1100-620 so that the effects of carbon content can be excluded.

No discernible differences were found between XRD patterns or TEM images of of Si-1100-800 (Figure S6 and Figure S7) and Si-1100-620 (Figures 1b and 3e). **Figure 5**a shows the Raman spectra of Si-1100-620 and Si-1100-800 in the wavenumber range containing carbon bands. Peaks around 1600 cm^{-1} and 1340 cm^{-1} are present for both composites and correspond to the G (graphitic) and D (disordered) bands of carbon, indicating that the carbon coatings are composed of amorphous carbon.[29] However, the D/G ratio of Si-1100-800 is estimated to be 2.1, lower than the 2.3 of Si-1100-620, which suggests a higher degree of graphization and a lower content of sp^3 carbon at higher deposition temperature.[48]

The influence of carbon deposition temperature on the underlying Si was investigated by performing X-ray

Table 1. Summary of building block size, surface area, reversible capacity, 1st cycle CE and cyclability of various Si–C composites.

Samples	Size of Si building blocks (nm)	Surface area[a] (m^2/g)	Reversible capacity of Si–C composite and Si alone (mAh/g)	1st cycle CE	Cyclability
Si-950-620[ref.[31]]	10	313	1544/1930	77%	Excellent
Si-1100-620	15	286	1962/2452	78%	Excellent
Si-1300-620	30	92	2253/2816	82%	Stable for 20 cycles
Si-1400-620	80	58	2778/3472	84%	Fading from the beginning

[a]N_2 sorption isotherms and pore size distribution are presented in Figure S3 in SI.

Adv. Energy Mater. **2013**,
DOI: 10.1002/aenm.201300496

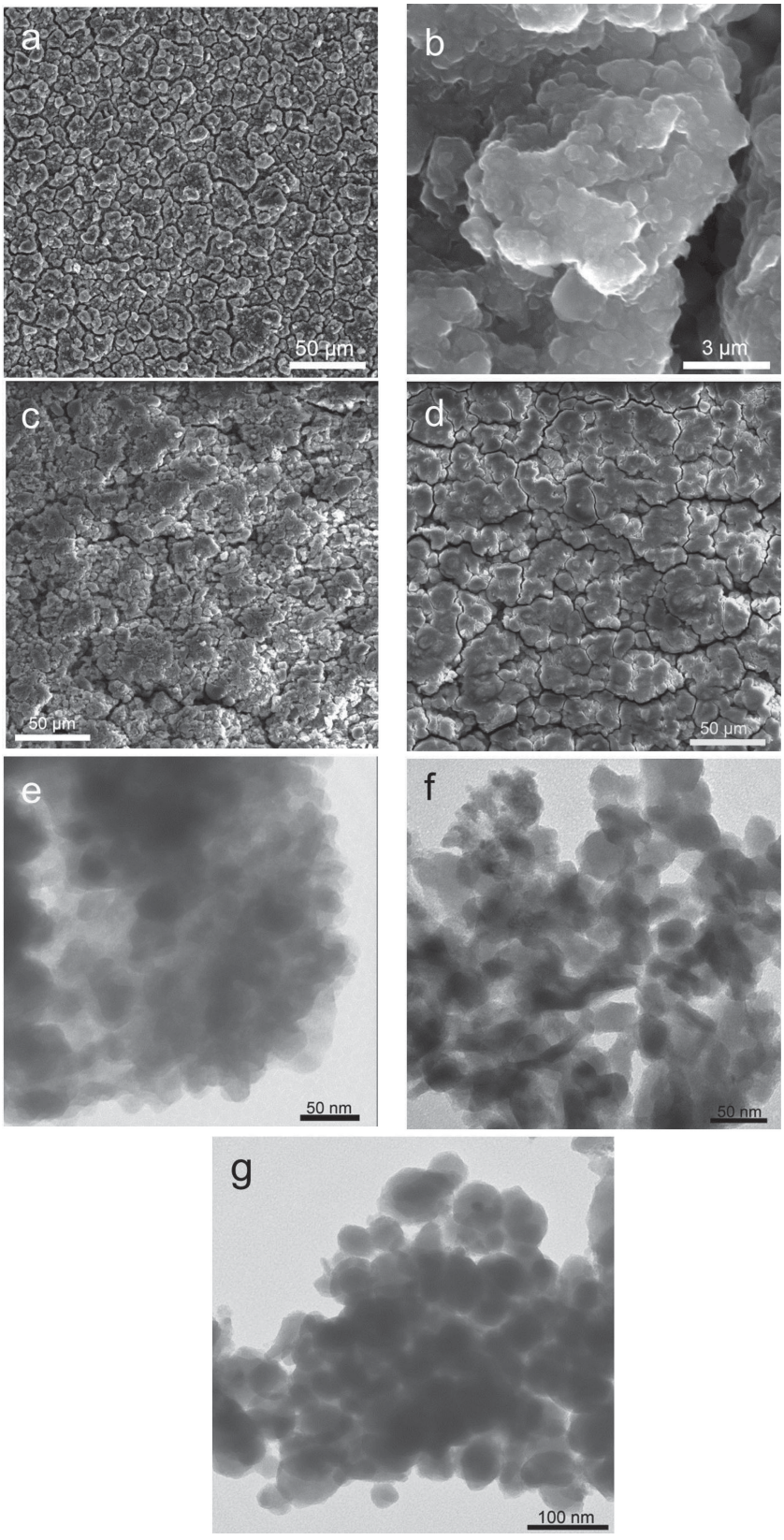

Figure 3. SEM images of electrodes with different Si–C composites after 100 cycles: (a) low and (b) high magnification images of Si-1100-620, (c) Si-1300-620, and (d) Si-1400-620. TEM images of different Si–C composites after 100 cycles: (e) Si-1100-620, (f) Si-1300-620, and (g) Si-1400-620.

photoelectron spectroscopy (XPS) on porous Si, Si-1100-620, and Si-1100-800, as shown in Figure 5b. The peaks around 99.5 eV and 103.4 eV are assigned to Si(0) and Si(4+), respectively, and the binding energies in between correspond to SiO_x ($0 < x < 2$).[11,49] The shift of Si(0) binding energy probably results from different oxidation state of materials.[50] It is clear that Si is partially oxidized after carbon coating even under Ar atmosphere (Grade 5.0 Ar is used), consistent with previous findings.[51] The key difference between Si-1100-620 and Si-1100-800 is that, as carbon coating temperature increases, the intensity of the SiO_x region decreases and the intensity of the Si(4+) peak (corresponding to SiO_2) increases relative to the intensity of the Si(0) peak, which may be due to disproportionation of SiO_x and/or its reduction by acetylene.[49] To determine whether overall oxide content increases or decreases (whether increase of SiO_2 or decrease of SiO_x is dominant), Raman spectra were collected for the three materials (Figure 5c). A strong peak at 510 cm^{-1} and two broad peaks around 300 and 935 cm^{-1} are observed for porous Si, corresponding to characteristic peaks of nanoscale Si.[52] Porous Si also shows a weak broad bump around 350 cm^{-1}, which is assigned to amorphous SiO_2 and SiO_x ($0 < x < 2$).[53] After carbon deposition at 620 °C, the peak corresponding to SiO_2 and SiO_x ($0 < x < 2$) becomes more prominent while the two broad peaks around 300 and 935 cm^{-1} become much weaker, which agrees well with the XPS results. However, with a carbon deposition temperature of 800 °C, the peak related to SiO_2 and SiO_x ($0 < x < 2$) can hardly be observed, indicating that the overall silicon oxide content decreases (decrease of SiO_x prevails over the increase of SiO_2). We propose that this difference results from the difference in competition between oxidation (by oxygen residue after purging with Ar and the miniscule amount of oxygen in the Ar itself) and reduction (by acetylene on the surface of Si) at different temperatures.[41,54] The porous Si tends to be partially oxidized by oxygen due to the relatively weak reducing ability of the acetylene when the temperature is low. At higher temperature, acetylene can partially reduce SiO_x to Si. The variance in reducing ability may be due to different decomposition mechanisms of acetylene at different temperatures, as described in previous work.[55]

The electrochemical performance of Si-1100-800 is shown in **Figure 6**. Si-1100-800 exhibits a 1st cycle CE of 86% (Figure 6a),

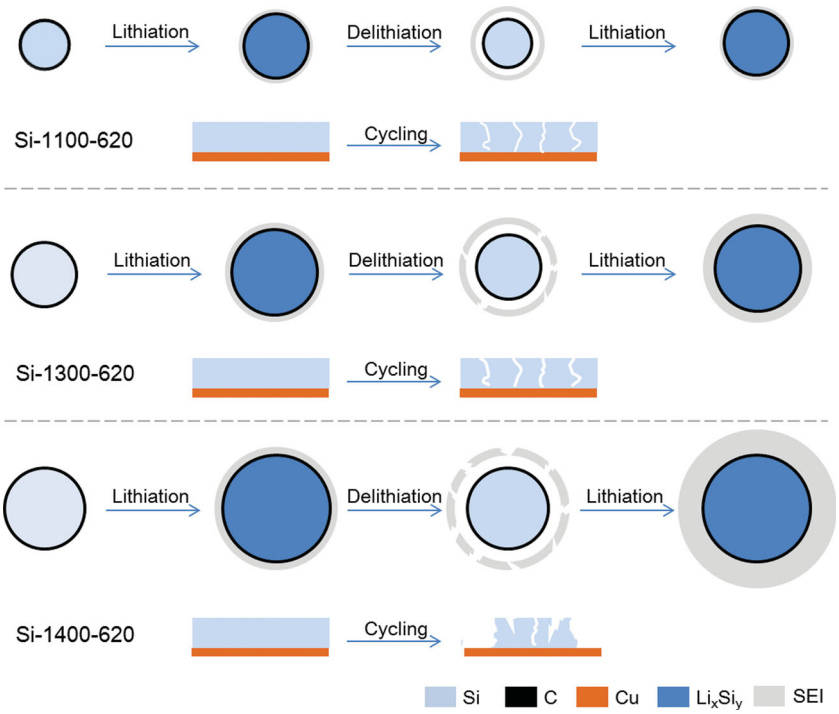

Figure 4. Scheme of evolution of SEI layer on Si building blocks and electrode structure of different micro-sized Si–C composites upon cycling.

which is much improved from the 78% 1st cycle CE of Si-1100-620, along with excellent capacity retention (Figure 6b) and initial discharge and charge capacities of 2250 and 1942 mAh/g, respectively. The rate performance of Si-1100-620 and Si-1100-800 were also studied. To examine the effect of carbon coating only, electrodes for the rate capability test were prepared without Super P carbon additive (Si–C composite and binder in an 8:2 ratio). As shown in Figure 6c, both of the electrodes have similar capacity retention at relatively low current densities. However, a noticeable difference was found at high rate. A capacity of 990 mAh/g was achieved at 6.4 A/g by Si-1100-800, corresponding to retention of 49% based on the capacity at 400 mA/g. In contrast, at the same current density, Si-1100-620 only delivered 610 mAh/g (a retention of 31%). This difference was further studied by electrochemical impedance spectroscopy (EIS) measurements (Figure 6d) on Si-1100-800 and Si-1100-620 cells after the rate capability test. The semicircle on the EIS spectrum of Si-1100-800 is smaller than that on the spectrum of Si-1100-620, indicating that Si-1100-800 has a lower charge transfer resistance.[56]

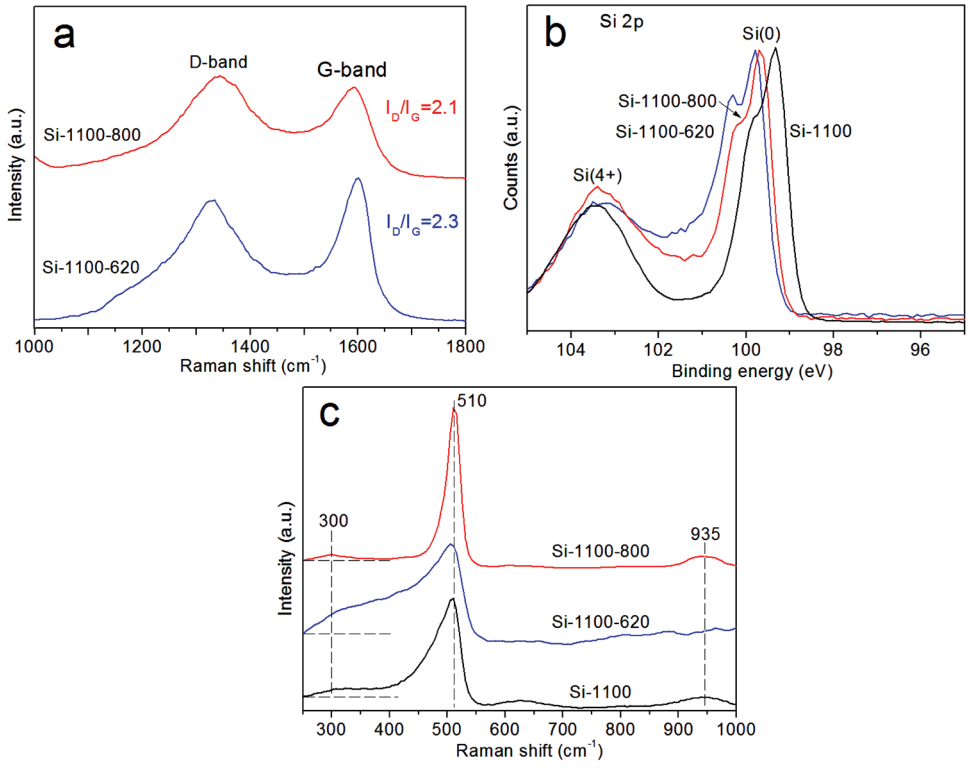

Figure 5. (a) Raman spectra of Si-1100-620 and Si-1100-800 around carbon region; (b) XPS spectra of Si-1100, Si-1100-620 and Si-1100-800; (c) Raman spectra of Si-1100, Si-1100-620 and Si-1100-800 around the silicon region.

DOI: 10.1002/aenm.201300496

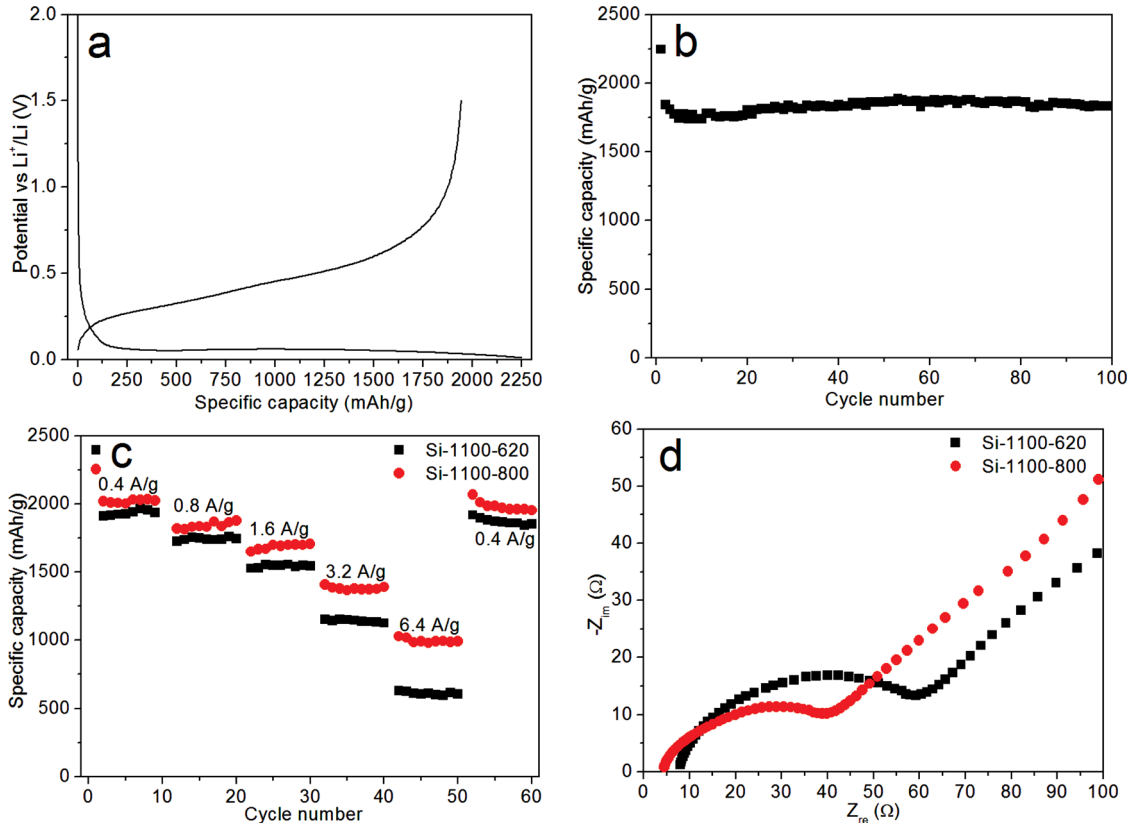

Figure 6. (a) First cycle voltage profile and (b) cycling performance of Si-1100-800 electrode. (c) Rate performance and (d) impedance spectra measured after rate capability test of Si-1100-620 and Si-1100-800 electrodes without Super P.

The improvement in both the 1st cycle CE and rate capability of Si-1100-800 can be attributed to the synergistic effect of better carbon quality and reduction of SiO_x at higher deposition temperature. Si-1100-800 has a more graphitic carbon coating, which helps to form a more compact SEI layer and thus achieve a higher CE.[57] In addition, with less SiO_x, the irreversible consumption of Li^+ by formation of Li_2O and Li_4SiO_4 should be lessened, giving a higher 1st CE. The enhanced rate performance of Si-1100-800 is attributed to the composite's higher electrical conductivity, which also comes from both reduction of SiO_x and improved carbon quality. Firstly, formation of less Li_2O and Li_4SiO_4 leads to lower resistance, as they are electrically insulating;[58,59] secondly, carbon formed at 800 °C has lower D/G ratio and higher sp^3 content and as a result has higher electronic conductivity,[42] agreeing well with the study on $LiFePO_4$/C composites that sp^2/sp^3 and D/G ratios closely correlate with electrochemical performance.[60] Previous investigation on carbon coating of multi-dimensional bulk Si anodes at different temperatures of 700, 900 and 1000 °C shows that carbon deposited at 900 °C has the highest degree of graphitization (D/G ratio of 2.1) and the resultant composite exhibits the best electrochemical performance.[23] Based on the current and previous findings, the upper limit of carbonization temperature should be in the range of 800 to 900 °C.

To demonstrate the long-term cyclability of the Si–C composites, the optimized Si-1100-800 was cycled with the fixed lithiation capacity of 1200 mAh/g at a rate of 1.2 A/g between 0.01 to 1.5V. These conditions were chosen because: 1) it has been demonstrated that the cycle life of Si-based anodes can be extended by controlling the amount of lithium that alloys with the silicon,[61,62] and 2) replacing the presently-used carbonaceous anodes with anodes having capacity on the order of 1000 to 1200 mAh/g would grant a significant improvement in the specific capacity of Li-ion batteries.[63,64] As shown in **Figure 7**a, the charge capacity was maintained well for 600 cycles. The first cycle CE is 81% and the average CE from the 2nd to the 600th cycle is 99.51%. Figure 7b plots the corresponding discharge–charge voltage profiles at different cycles, which remain similar in shape aside from the lithiation voltage slowly decreasing. As far as we know, this is the best cycling performance with such a high capacity for micro-sized Si-based anodes.[65]

3. Conclusion

In summary, the Si building block size of micro-sized Si–C composites has been effectively controlled by varying the disproportionation temperature of the SiO precursor, and its influence on electrochemical performance of the composites has been investigated. The 1st cycle coulombic efficiency and reversible capacity of the Si–C composites increase as building

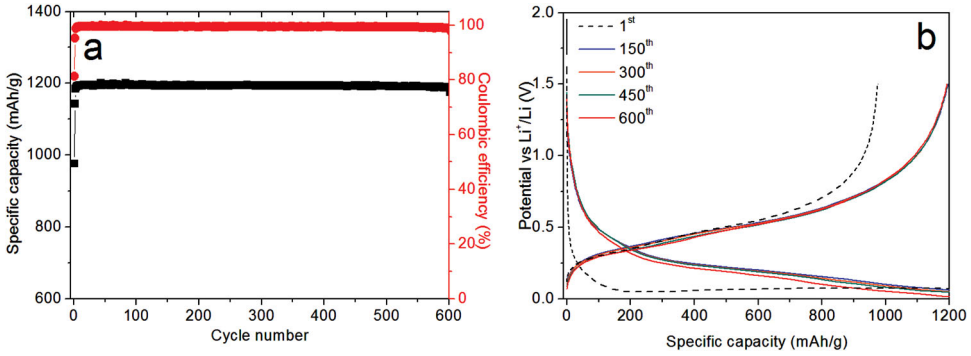

Figure 7. (a) The cycling performance and (b) voltage profiles of Si-1100-800 electrode with a constant discharge (lithiation) capacity of 1200 mAh/g between 1.5 to 0.01V at 1.2 A/g after first six cycles activated at 600 mA/g.

block size increases, while cycling stability plummets. 15 nm was found to be the critical size that enables both high reversible capacity and excellent cycling stability. The 1st cycle CE and high rate performance can be greatly improved by carbon coating at a higher temperature of 800 °C, because more SiO_x ($0 < x < 2$) is reduced and carbon of better quality is formed. Stable cycling for 600 cycles at a rate of 1.2 A/g with a fixed lithiation capacity of 1200 mAh/g was achieved by the micro-sized Si–C composite prepared with the optimized nanoscale building block size and carbon coating temperature. We expect that the present findings will aid future design and preparation of high-performance micro-sized Si–C composites.

4. Experimental Section

Synthesis of Micro-Sized Si–C Composites: The preparation procedures of porous Si are the same as our previous report except for different thermal disproportionation temperature.[31] Three different temperatures of 1100, 1300 and 1400 °C were used and the corresponding products are designated Si-1100, Si-1300 and Si-1400, respectively. Carbon coating of porous Si was done by thermal decomposition of acetylene gas at 620 °C and 800 °C (for Si-1100 only) in a quartz furnace. The mixture of acetylene and high-purity argon (argon: acetylene = 9:1 by volume) is introduced at different flow rates for different duration to make all final Si–C composites have similar carbon content. The resultant products are designated Si-1100-620 and Si-1100-800, respectively.

Characterization: The obtained samples were characterized on a Rigaku Dmax-2000 X-ray powder diffractometer (XRD) with Cu Kα radiation (λ = 1.5418 Å). The operation voltage and current were kept at 40 kV and 30 mA, respectively. The size and morphology of the as-synthesized products were determined by a JEOL-1200 transmission electron microscope (TEM), FEI Nova NanoSEM 630 scanning electron microscope (SEM). The Brunauer–Emmett–Teller (BET) specific surface area of the samples was determined by a Micrometrics ASAP 2020 physisorption analyzer using the standard N_2 adsorption and desorption isotherm measurements at 77 K. X-ray photoelectron spectroscopy (XPS) was conducted with a Kratos Analytical Axis Ultra XPS. Raman spectroscopy was conducted with a WITec CMR200 confocal Raman instrument.

Electrochemical Measurements: The electrochemical experiments were performed using 2016-type coin cells, which were assembled in an argon-filled dry glovebox (MBraun, Inc.) with carbon-coated Si electrode as the working electrode and the Li metal as the counter electrode. The working electrodes, except for those used in rate capability test, were prepared by casting the slurry consisting of 60 wt% of active material, 20 wt% of Super P carbon black, and 20 wt% of poly(acrylic acid) (PAA) binder. The working electrodes for postmortem TEM analysis and rate capability test were prepared by casting the slurry consisting of 80 wt% of active material and 20 wt% of poly(acrylic acid) (PAA) binder without Super P carbon black. The mass loading on each electrode is about 2 mg/cm^2. 1 mol/L LiPF6 in a mixture of ethylene carbonate, diethyl carbonate and dimethyl carbonate (EC: DEC: DMC, 2:1:2 by vol%) and 10 wt% fluoroethylene carbonate (FEC) was used as the electrolyte (Novolyte Technologies, Independence, OH). The electrochemical performance was evaluated by galvanostatic charge/discharge cycling on an Arbin BT-2000 battery tester at room temperature under different current densities in the voltage range between 1.5 and 0.01 V versus Li^+/Li. The current density and specific capacity are calculated based on the mass of carbon-coated Si composite.

Supporting Information

Supporting Information is available from the Wiley Online Library or from the author.

Acknowledgements

This work was supported by the Assistant Secretary for Energy Efficiency and Renewable Energy, Office of Vehicle Technologies of the U.S. Department of Energy under Contract No. DE-AC02-05CH11231, Subcontract NO. 6951378 under the Batteries for Advanced Transportation Technologies (BATT) Program.

Received: May 8, 2013
Revised: May 28, 2013
Published online:

[1] M. S. Whittingham, *Chem. Rev.* **2004**, *104*, 4271.
[2] B. Kang, G. Ceder, *Nature* **2009**, *458*, 190.
[3] M. Armand, J. M. Tarascon, *Nature* **2008**, *451*, 652.
[4] M. Winter, J. O. Besenhard, M. E. Spahr, P. Novák, *Adv. Mater.* **1998**, *10*, 725.
[5] B. A. Boukamp, G. C. Lesh, R. A Huggins, *J. Electrochem. Soc.* **1981**, *128*, 725.
[6] H. Wu, G. Chan, J. W. Choi, I. Ryu, Y. Yao, M. T. McDowell, S. W. Lee, A. Jackson, Y. Yang, L. Hu, Y. Cui, *Nat. Nanotechnol.* **2012**, *7*, 310.
[7] L. Y. Beaulieu, K. W. Eberman, R. L. Turner, L. J. Krause, J. R. Dahn, *Electrochem. Solid-State Lett.* **2001**, *4*, A137.
[8] S. R. Chen, M. L. Gordin, R. Yi, G. Howlett, H. Sohn, D. H. Wang, *Phys. Chem. Chem. Phys.* **2012**, *14*, 12741.

[9] W. Wang, P. N. Kumta, *ACS Nano* **2010**, *4*, 2233.
[10] H. Wu, G. Zheng, N. Liu, T. J. Carney, Y. Yang, Y. Cui, *Nano Lett.* **2012**, *12*, 904.
[11] N. Liu, H. Wu, M. T. McDowell, Y. Yao, C. Wang, Y. Cui, *Nano Lett.* **2012**, *12*, 3315.
[12] L. F. Cui, Y. Yang, C. M. Hsu, Y. Cui, *Nano Lett.* **2009**, *9*, 3370.
[13] W. Zhou, S. Upreti, M. S. Whittingham, *Electrochem. Commun.* **2011**, *13*, 1102.
[14] M. Holzapfel, H. Buqa, W. Scheifele, P. Novák, F. M. Petrat, *Chem. Commun.* **2005**, 1566.
[15] J. K. Lee, K. B. Smith, C. M. Hayner, H. H. Kung, *Chem. Commun.* **2010**, *46*, 2025.
[16] J. K. Yoo, J. Kim, Y. S. Jung, K. Kang, *Adv. Mater.* **2012**, *40*, 5452.
[17] L. Su, Y. Jing, Z. Zhou, *Nanoscale* **2011**, *3*, 3967.
[18] C. K. Chan, H. Peng, G. Liu, K. McIlwrath, X. F. Zhang, R. A. Huggins, Y. Cui, *Nat. Nanotechnol.* **2008**, *3*, 31.
[19] X. Chen, K. Gerasopoulos, J. Guo, A. Brown, C. Wang, R. Ghodssi, J. N. Culver, *ACS Nano* **2010**, *4*, 5366.
[20] J. H. Warner, A. Hoshino, K. Yamamoto, R. D. Tilley, *Angew. Chem. Int. Ed.* **2005**, *44*, 4550.
[21] H. Kim, B. Han, J. Choo, J. Cho, *Angew. Chem. Int. Ed.* **2008**, *47*, 10151.
[22] A. Magasinski, P. Dixon, B. Hertzberg, A. Kvit, J. Ayala, G. Yushin, *Nat. Mater.* **2010**, *9*, 353.
[23] B. M. Bang, H. Kim, H. K. Song, J. Cho, S. Park, *Energy Environ. Sci.* **2011**, *4*, 5013.
[24] B. M. Bang, J. I. Lee, H. Kim, J. Cho, S. Park, *Adv. Energy Mater.* **2012**, *2*, 878.
[25] J. I. Lee, S. Park, *Nano Energy* **2013**, *2*, 146.
[26] G. Jeong, J. H. Kim, Y. U. Kim, Y. J. Kim, *J. Mater. Chem.* **2012**, *22*, 7999.
[27] J. H. Kim, H. J. Sohn, H. Kim, G. Jeong, W. Choi, *J. Power Sources* **2007**, *170*, 456.
[28] T. Morita, N. Takami, *J. Electrochem. Soc.* **2006**, *153*, A425.
[29] J. I. Lee, N. S. Choi, S. Park, *Energy Environ. Sci.* **2012**, *5*, 7878.
[30] J. I. Lee, K. T. Lee, J. Cho, J. Kim, N. S. Choi, S. Park, *Angew. Chem. Int. Ed.* **2012**, *51*, 2767.
[31] R. Yi, F. Dai, M. L. Gordin, S. R. Chen, D. H. Wang, *Adv. Energy Mater.* **2013**, *3*, 295.
[32] F. Dai, R. Yi, M. L. Gordin, S. R. Chen, D. H. Wang, *RSC Adv.* **2012**, *2*, 12710.
[33] H. Kim, M. Seo, M. H. Park, J. Cho, *Angew. Chem. Int. Ed.* **2010**, *49*, 2146.
[34] M. T. McDowell, S. W. Lee, I. Ryu, H. Wu, W. D. Nix, J. W. Choi, Y. Cui, *Nano Lett.* **2011**, *11*, 4018.
[35] I. Ryu, J. W. Choi, Y. Cui, W. D. Nix, *J. Mech. Phys. Solids* **2011**, *59*, 1717.
[36] Y. C. Yen, S. C. Chao, H. C. Wu, N. L. Wu, *J. Electrochem. Soc.* **2009**, *156*, A95.
[37] Y. H. Xu, G. P. Yin, Y. L. Ma, P. J. Zuo, X. Q. Chen, *J. Mater. Chem.* **2010**, *20*, 3216.
[38] Y. S. Hu, R. Demir-Cakan, M. M. Titirici, J. O. Müller, R. Schlögl, M. Antonietti, J. Maier, *Angew. Chem. Int. Ed.* **2008**, *47*, 1645.
[39] K. Evanoff, A. Magasinski, J. B. Yang, G. Yushin, *Adv. Energy Mater.* **2011**, *1*, 495.
[40] H. P. Jia, P. F. Gao, J. Yang, J. L. Wang, Y. N. Nuli, Z. Yang, *Adv. Energy Mater.* **2011**, *1*, 1036.
[41] K. H. Seng, M. H. Park, Z. P. Guo, H. K. Liu, J. Cho, *Nano Lett.* **2013**,*13*, 1230.
[42] J. D. Wilcox, M. M. Doeff, M. Marcinek, R. Kostecki, *J. Electrochem. Soc.* **2007**, *154*, A389.
[43] X. L. Li, P. Meduri, X. L. Chen, W. Qi, M. H. Engelhard, W. Xu, F. Ding, J. Xiao, W. Wang, C. M. Wang, J. G. Zhang, J. Liu, *J. Mater. Chem.* **2012**, *22*, 11014.
[44] M. T. McDowell, S. W. Lee, I. Ryu, H. Wu, W. D. Nix, J. W. Choi, Y. Cui, *Nano Lett.* **2011**, *11*, 4018.
[45] P. R. Abel, Y. M. Lin, H. Celio, A. Heller, C. B. Mullins, *ACS Nano*, **2012**, *6*, 2506.
[46] M. T. McDowell, S. W. Lee, J. T. Harris, B. A. Korgel, C. Wang, W. D. Nix, Y. Cui, *Nano Lett.* **2013**, *13*, 758.
[47] X. H. Liu, L. Zhong, S. Huang, S. X. Mao, T. Zhu, J. Y. Huang, *ACS Nano* **2012**, *6*, 1522.
[48] N. Shimodaira, A. Masui, *J. Appl. Phys.* **2002**, *92*, 902.
[49] D. Gautam, E. Koyanagi, T. Uchino, *J. Appl. Phys.* **2009**, *105*, 073517.
[50] F. Jolly, F. Rochet, G. Dufour, C. Grupp, A. Taleb-Ibrahimi, *J. Non-Cryst. Solids* **2001**, *280*, 150.
[51] J. Lee, J. Bae, J. Heo, I. T. Han, S. N. Cha, D. K. Kim, M. Yang, H. S. Han, W. S. Jeon, J. Chung, *J. Electrochem. Soc.* **2009**, *156*, A905.
[52] R. Wang, G. Zhou, Y. Liu, S. Pan, H. Zhang, D. Yu, Z. Zhang, *Phys. Rev. B* **2000**, *61*, 16827.
[53] S. Hernández, A. Martínez, P. Pellegrino, Y. Lebour, B. Garrido, E. Jordana, J. M. Fedeli, *J. Appl. Phys.* **2008**, *104*, 044304.
[54] K. H. Seng, M. H. Park, Z. P. Guo, H. K. Liu, J. Cho, *Angew. Chem. Int. Ed.* **2012**, *51*, 5657.
[55] T. Tanzawa, W. C. Gardiner Jr., *J. Phys. Chem.* **1980**, *84*, 236.
[56] E. Pollak, G. Salitra, V. Baranchugov, D. Aurbach, *J. Phys. Chem. C* **2007**, *111*, 11437.
[57] C. Natarajan, H. Fujimoto, K. Tokumitsu, A. Mabuchi, T. Kasuh, *Carbon* **2001**, *39*, 1409.
[58] M. Tatsumisago, H. Yamashita, A. Hayashi, H. Morimoto, T. Minami, *J. Non-Cryst. Solids* **2000**, *274*, 30.
[59] C. Wang, A. J. Appleby, F. E. Little, *Solid State Ionics* **2002**, *147*, 13.
[60] M. M. Doeff, J. D. Wilcox, R. Yu, A. Aumentado, M. Marcinek, R. Kostecki, *J. Solid State Electrochem.* **2008**, *12*, 995.
[61] L. F. Cui, L. Hu, H. Wu, J. W. Choi, Y. Cui, *J. Electrochem. Soc.* **2011**, *158*, A592.
[62] M. N. Obrovac, L. J. Krause, *J. Electrochem. Soc.* **2007**, *154*, A103.
[63] M. Yoshio, T. Tsumura, N. Dimov, *J. Power Sources* **2005**, *146*, 10.
[64] U. Kasavajjula, C. Wang, A. J. Appleby, *J. Power Sources* **2007**, *163*, 1003.
[65] M. Thakur, S. L. Sinsabaugh, M. J. Isaacson, M. S. Wong, S. L. Biswal, *Sci. Rep.* **2012**, *2*, 795.